Short-Range Leakage Cancelation in FMCW Radar Transceivers Using an Artificial On-Chip Target

Alexander Melzer, *Student Member, IEEE*, Alexander Onic, *Member, IEEE*, Florian Starzer, and Mario Huemer, *Senior Member, IEEE*

***Abstract*—A major drawback of frequency modulated continuous-wave (FMCW) radar systems is the permanent leakage from the transmit into the receive path. Besides leakage within the radar device itself, signal reflections from a fixed object in front of the antennas additionally introduce so-called short-range (SR) leakage. It causes a strong degradation of detection sensitivity due to the unpreventable phase noise of the transmit oscillator. In this work, we introduce an artificial on-chip target (OCT) to mitigate the SR leakage. The OCT consists of a delay line whose time delay is significantly smaller than the round-trip delay time of the SR leakage. This is motivated by the fact that in integrated circuits for automotive radar applications operating at 77 GHz delay lines in the range of only a few picoseconds can be realized with a reasonable amount of circuitry. Despite this constraint, we show that the proposed method achieves almost perfect cancelation of the SR leakage. The concept is based on the cross-correlation properties of the residual phase noise in the intermediate frequency (IF) domain. Further, the effectiveness of the proposed method is verified in an FMCW radar system simulation. It almost perfectly shows that a gain in sensitivity of approximately 6 dB is achieved, compensating for the performance degradation caused by the SR leakage. The novel leakage cancelation concept is carried out mainly in the digital domain enabling high flexibility and adaptivity.**

***Index Terms*—Digital signal processing, frequency modulated continuous-wave (FMCW) radar, leakage cancelation, phase noise, reflected power canceler.**

I. Introduction

FREQUENCY modulated continuous-wave (FMCW) radar systems have a wide application range for distance and velocity measurements and are seamlessly integrated in todays' environment. Different to pulse based radar systems, an FMCW radar uses a linear chirp sequence as transmit signal. The signals reflected by the radar targets are mixed with the instantaneous transmit signal and filtered to remove the image. For a single static object this results in a sinusoidal signal with constant frequency, termed *beat frequency*, which is directly proportional to the target distance. In order to detect several targets, the frequency spectrum of the intermediate frequency (IF) domain is estimated.

Even though the instantaneous transmit power can be significantly reduced compared to pulse radar, FMCW radar suffers from permanent leakage from the transmit into the receive path [1]–[3]. This becomes even more crucial when implementing the radar in an integrated circuit (IC), where isolation is limited. This on-chip leakage signal is mixed in the same manner as the reflections from the targets. Due to its small propagation delay a beat frequency close to DC is generated in the IF domain, which is why it is well known as the *DC offset issue*. Cancelation techniques for the DC offset issue have gained significant interest. In [2], [4] a heterodyne scheme is utilized to isolate the mixer noise from the leakage signal in order to extract the interference signal. A similar concept is proposed in [5], where the heterodyne reference signal is generated in the digital domain.

The issue of leakage is well known also in many other fields, such as communications engineering. For instance, in [6] a leakage canceler for an RFID reader implemented on a single chip is proposed. Differently, [7], [8] proposes a concept to cancel second-order intermodulation products originating from the portion of the transmit signal leaking into the receive path in UMTS and LTE transceivers. The proposed methods partly employ similar concepts for leakage cancelation as compared to such that cancel the DC offset issue in FMCW radar systems [2], [3].

Different to the typical leakage on chip, in this work a fixed but significantly disturbing object in front of the radar antennas is considered. We aim to cancel its signal reflections in the digital IF domain. These reflections are introduced as *short-range (SR) leakage*. The application that we target is an automotive radar system, where transmit and receive antennas are mounted right behind the bumper, which is the source of the unwanted signal reflection.

The issue of SR leakage is similar to that of the DC offset problem, however two essential differences arise. Firstly, the reflected signals from the SR target are in general of significantly higher amplitude. That is due to the fact that the SR target is considered to be only in a few centimeters distance from the radar antennas such that the transmit to receive signal power ratio is less than the achievable isolation inside the radar device. Secondly, due to the increased propagation delay, i.e., two times the time-of-flight of the radio waves to the SR target, the residual phase noise (PN) after mixing becomes a dominant noise term. This phenomenon is well known as *range correlation effect* [9] in the radar literature and is comparably small for the DC offset problem due to the negligibly small propagation delay.

Potential cancelation techniques for the SR leakage commonly introduce a radar reference path. This path consists in

Manuscript received January 30, 2015; revised May 11, 2015; accepted July 21, 2015. Date of publication August 05, 2015; date of current version November 17, 2015. This work was supported by the Austrian Center of Competence in Mechatronics (ACCM) . The guest editor coordinating the review of this manuscript and approving it for publication was Dr. Yuri Abramovich.

A. Melzer and M. Huemer are with the Institute of Signal Processing, Johannes Kepler University Linz, 4040 Linz, Austria (e-mail: alexander.melzer@jku.at; mario.huemer@jku.at).

A. Onic and F. Starzer are with DICE Danube Integrated Circuit Engineering GmbH & Co. KG, 4040 Linz, Austria (e-mail: alexander.onic@infineon.com; florian.starzer@infineon.com).

Color versions of one or more of the figures in this paper are available online at http://ieeexplore.ieee.org.

Digital Object Identifier 10.1109/JSTSP.2015.2465298

1932-4553 © 2015 IEEE. Translations and content mining are permitted for academic research only. Personal use is also permitted, but republication/redistribution requires IEEE permission. See http://www.ieee.org/publications_standards/publications/rights/index.html for more information.

essence of a delay line that imitates the round trip delay time (RTDT) of the radar waves of a certain target in the channel. The *Reflected Power Canceler* (RPC) introduced in [10] claims to cancel reflections from a single target. This is achieved by adjusting the delay of the reference path such that it matches the RTDT of the unwanted target. Different to the problem at hand, the system is built with discrete components, allowing for a wide range for the delay. In [11], [12] the delay is realized with surface acoustic wave (SAW) technology. However, since the SAW technology has a transit frequency in the low GHz range, an additional local oscillator is required to downconvert the actual radar transmit signal.

In this work we introduce an artificial *on-chip target* (OCT) that emulates a radar target, and utilize it for SR leakage cancelation. We put emphasis on the so called *decorrelated phase noise* (DPN) that is introduced as part of the downconversion process and severely deteriorates the target detection sensitivity. Equivalently to the RPC in [10], the OCT consists of a delay line. However, within a *Monolithic Microwave Integrated Circuit* (MMIC) operating at 77 GHz, delay lines can only be implemented as a fraction of the RTDT of the SR leakage with reasonable amount of circuit size. Despite this design constraint in MMICs, our proposed concept achieves almost perfect cancelation of the SR leakage.

Since the actual leakage cancelation is performed in the digital IF domain, the amount of analog circuitry is reduced to a few blocks. There are no additional vector modulators or even reference oscillators required. Further, the cancelation concept can be configured for different hardware setups and is adaptable to changes of the SR leakage over time.

The paper is structured as follows. Section II introduces the used FMCW radar system model as well as the on-chip target. Cross-correlation properties from two DPN terms are evaluated in Section III. Based on these correlation properties, Section IV proposes the actual leakage cancelation concept carried out in the digital domain. Finally, in Section V we verify our analytical derivations carrying out a full FMCW radar simulation with the proposed concept.

II. System Model

In this section the radar system model under consideration (Fig. 1) is defined and the analog IF signal is derived. Then, the impact of the SR leakage on the overall system performance is evaluated. Further, the *on-chip target* is introduced.

A. Transmit Signal

In order to derive the IF signal we first define the chirp used as transmit signal, which is a linear frequency ramp, given as

$$s(t) = A\cos\left(2\pi f_0 t + \pi k t^2 + \varphi(t) + \Phi\right) \tag{1}$$

for $t \in [0, T]$, where T is the duration of a single chirp. The chirp amplitude and start frequency are A and f_0, $k = B/T$ is the slope of the chirp with bandwidth B, $\varphi(t)$ is the PN introduced by the PLL and Φ is a constant phase. While e.g., in [1] non-linear frequency ramps are used, here we consider a linear frequency ramp only.

B. Receive Signal

The transmit signal is fed into the channel which comprises of two sources of signal reflections. Firstly, the targets that are to be detected and its distances to be estimated. They are modeled with a delay τ_{Tm} and a gain A_{Tm}, where $m = 1 \ldots M$ and M is the number of targets. Secondly, the SR leakage representing the unwanted close signal reflections. Analogous to a target in open field it is represented with a delay τ_S and gain A_S. We assume A_S to be typically significantly larger than any target reflection gain A_{Tm} as the SR leakage originates from reflections close to the radar antennas.

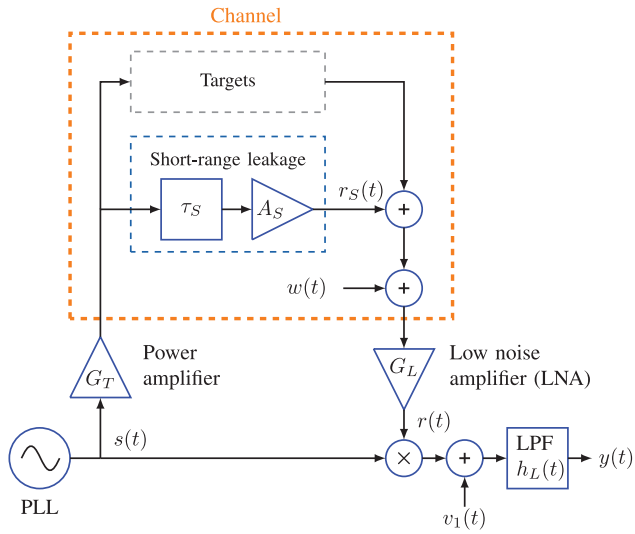

Fig. 1. FMCW radar system model consisting of a channel with M targets and the SR leakage. The reflected waves from the channel are downconverted with the instantaneous transmit signal. Lowpass filtering (LPF) this downconverted signal removes the image and reveals the analog IF signal $y(t)$.

At the receiver side additive white Gaussian noise (AWGN) is added before downconversion to the IF is carried out. In conclusion, the receive signal follows as

$$r(t) = \underbrace{A'_S\, s(t-\tau_S)}_{\text{SR leakage}} + \underbrace{\sum_{m=1}^{M} A'_{Tm}\, s(t-\tau_{Tm})}_{\text{Target reflections}} + \underbrace{G_L w(t)}_{\text{AWGN}}, \tag{2}$$

where the gains of the SR leakage and the targets are $A'_S = G_T A_S G_L$ and $A'_{Tm} = G_T A_{Tm} G_L$. Further, G_T and G_L determine the gains of the transmit power amplifier and the receive low noise amplifier (LNA), respectively.

C. Downconversion

Downconversion is employed by multiplying the instantaneous transmit signal $s(t)$ with the receive signal $r(t)$. A subsequent lowpass filter (LPF) removes the image originating from the mixing process and acts as anti-aliasing filter for the subsequent A/D conversion. For simplicity let $\Phi = 0$ such that after lowpass filtering with the impulse response $h_L(t)$ the IF signal becomes

$$\begin{aligned} y(t) &= \left[s(t)\, r(t) + v_1(t)\right] * h_L(t) \\ &= \frac{A^2 A'_S}{2}\cos\left(2\pi f_{BS} t + \Phi_S + \varphi(t) - \varphi(t-\tau_S)\right) \\ &\quad + \sum_{m=1}^{M} \frac{A^2 A'_{Tm}}{2}\cos(2\pi f_{BTm} t + \Phi_{Tm} + \varphi(t) - \varphi(t-\tau_{Tm})) \\ &\quad + w_L(t) + v_{1L}(t), \end{aligned} \tag{3}$$

where $*$ denotes the convolution operator. The beat frequencies are $f_{BS} = k\tau_S$ and $f_{BTm} = k\tau_{Tm}$, furthermore the constant phase terms follow as $\Phi_S = 2\pi f_0 \tau_S - k\pi\tau_S^2$ and $\Phi_{Tm} = 2\pi f_0 \tau_{Tm} - k\pi\tau_{Tm}^2$. The channel noise $w(t)$ and the intrinsic noise $v_1(t)$ are modeled as white Gaussian noise processes. Their respective contributions to the IF signal are $w_L(t) = [s(t)\, G_L\, w(t)] * h_L(t)$ and $v_{1L}(t) = v_1(t) * h_L(t)$.

D. Short-Range Leakage Analysis

We now analyze the SR leakage contribution to the overall IF signal, which from (3) is

$$y_S(t) = \underbrace{\frac{A^2 A'_S}{2}}_{\text{gain}} \cdot \cos\left(2\pi \underbrace{f_{BS}}_{\text{beat freq.}} t + \underbrace{\Phi_S}_{\text{const. phase}} + \underbrace{\varphi(t) - \varphi(t-\tau_S)}_{\Delta\varphi_S(t),\ \text{DPN}}\right) \tag{4}$$

The gain in (4) is determined by the *radar cross section* of the SR target and decays rapidly with the distance. Therefore, A_S is in general larger than any A_{Tm}. The beat frequency depends on the sweep slope k of the chirp and the RTDT τ_S. The latter is proportional to the distance of the SR target $d_S = \tau_S c/2$, with the speed of light c.

The DPN term $\Delta\varphi_S(t)$ in (4) acts as noise source. With increasing distance and therefore larger RTDT, the PN $\varphi(t)$ differs more and more from the delayed PN $\varphi(t-\tau_S)$. This phenomenon is termed *range correlation effect* [9] in the literature and the difference $\varphi(t) - \varphi(t-\tau_S)$ is termed *decorrelated phase noise* (DPN). Note that for the DC offset issue the DPN is less of an issue as the corresponding delay is very small.

To further analyze its impact on the IF signal we apply the cosine sum identity to (4), that is

$$y_S(t) = \frac{A^2 A'_S}{2}\cos(2\pi f_{BS} t + \Phi_S)\cos(\Delta\varphi_S(t)) - \frac{A^2 A'_S}{2}\sin(2\pi f_{BS} t + \Phi_S)\sin(\Delta\varphi_S(t)). \tag{5}$$

Assuming $\Delta\varphi_S(t)$ to be sufficiently small (e.g., with $\tau_S = 800\,\text{ps}$ we have $|\Delta\varphi_S(t)| < 0.03$ for the exemplary PN power spectrum from Fig. 2) allows for the approximations $\cos(\Delta\varphi_S(t)) \approx 1$ and $\sin(\Delta\varphi_S(t)) \approx \Delta\varphi_S(t)$, such that (5) approximates to

$$y_S(t) \approx \frac{A^2 A'_S}{2}\cos(2\pi f_{BS} t + \Phi_S) - \frac{A^2 A'_S}{2}\sin(2\pi f_{BS} t + \Phi_S)\,\Delta\varphi_S(t). \tag{6}$$

To analyze the impact of the DPN $\Delta\varphi_S(t)$ on the IF signal, we regard its power spectrum, which is given as [9]

$$S_{\Delta\varphi_S\Delta\varphi_S}(f) = 2\, S_{\varphi\varphi}(f)\,(1 - \cos(2\pi f \tau_S)), \tag{7}$$

where $S_{\varphi\varphi}(f)$ is the power spectrum of the PN. The individual contributions as well as the resulting DPN power spectrum $S_{\Delta\varphi_S\Delta\varphi_S}(f)$ from (7) are depicted in Fig. 2 for an RTDT of $\tau_S = 800$ ps (or an equivalent distance of $d_S \approx 12\,\text{cm}$). Exemplarily, a typical PN power spectrum of a 77 GHz PLL is used here. For IF frequencies larger than 100 kHz, i.e., the frequency range of interest, the power spectrum $S_{\Delta\varphi_S\Delta\varphi_S}(f)$ is around $-140\,\text{dBc/Hz}$.

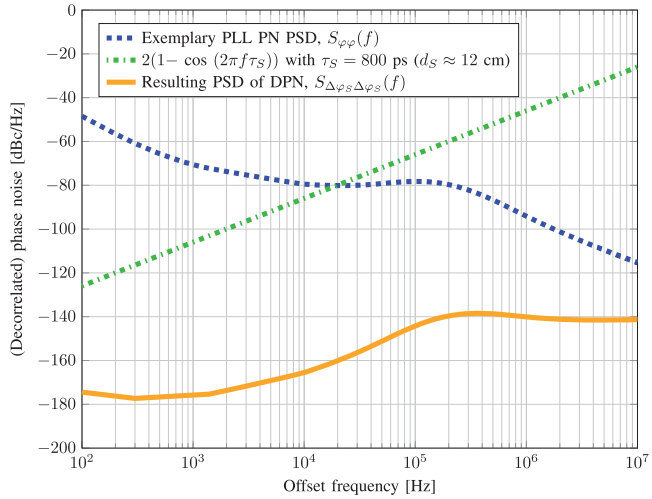

Fig. 2. Typical PLL PN power spectrum, range correlation effect, and resulting power spectrum from the SR leakage for $\tau_S = 800$ ps, or distance $d_S \approx 12$ cm.

The DPN $\Delta\varphi_S(t)$ is assumed to be statistically uncorrelated with other noise sources in the system. Therewith, the SR leakage affects the sensitivity of the radar device if the second summand in (6), that is the DPN error term in $y_S(t)$, is in the range or larger than the sum of the AWGN and the intrinsic noise power. The PSDs of the AWGN $w_L(t)$ and the intrinsic noise $v_{1L}(t)$ are given by $S_{w_L w_L}(f)$ and $S_{v_{1L} v_{1L}}(f)$, respectively.

As anticipated the critical configuration of the SR leakage depends on the phase noise, the system parameters A, G_T and G_L as well as the SR leakage parameters A_S and τ_S [13]. Clearly, if these parameters do not lead to an increased noise floor the proposed leakage canceler is not required.

A practical example is considered with a PLL output power of 0 dBm, i.e., $A = 0.316$ V with an impedance of $R = 50\,\Omega$. Further we assume a transmit power gain of $G_T = 10$ dB, a reflection factor of $A_S = -8$ dB, an LNA gain of $G_L = 20$ dB and a delay $\tau_S = 1$ ns. At an offset frequency of 1 MHz, where the exemplary PSD from Fig. 2 is $-94.15\,\text{dBc/Hz}$, the resulting DPN power is $-132.2\,\text{dBm/Hz}$. From measurements with existing MMICs and the parameters from above, the noise floor is known to be at $-140\,\text{dBm/Hz}$ in the IF domain. This results in a difference of 7.8 dB and consequently deteriorates the target detection sensitivity notably.

This observation motivates cancelation of the SR leakage, as its DPN increases the noise floor in the IF signal. Note that since for the DC offset issue the propagation delay is comparably small, its DPN contribution to the IF signal is negligible and therefore ignored in this work.

E. Artificial On-Chip Target for Short-Range Leakage Cancelation

We extend the system model in Fig. 1 by introducing an artificial *on-chip target* (OCT). The reader may already refer to Fig. 7 to see how it is integrated in the system model for leakage cancelation. As for the targets, it is modeled by a delay τ_O and a gain A_O, hence emulating a radar target. Equivalent to the

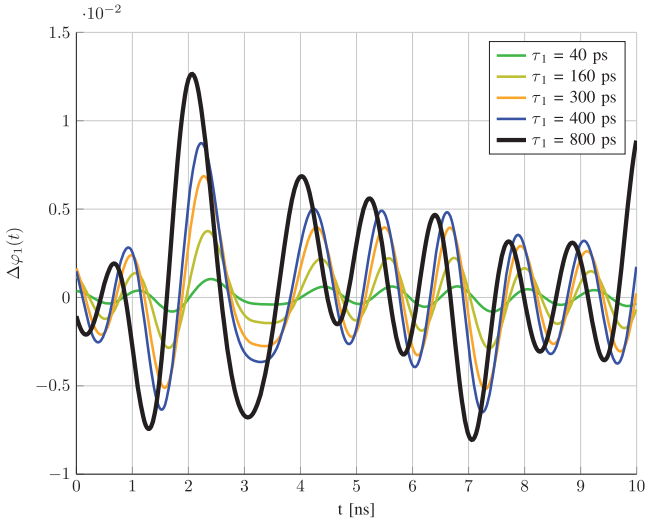

Fig. 3. Decorrelated phase noise for different delays τ_1 for a realization of the PN $\varphi(t)$ over 10 ns.

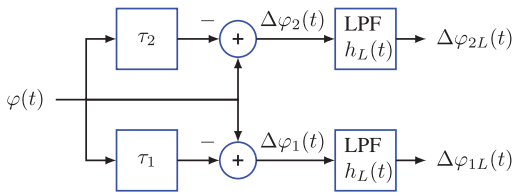

Fig. 4. Model utilized to analyze and compare two DPN terms.

channel, the OCT is fed by the chirp signal $s(t)$ and downconverted with the instantaneous transmit signal. The resulting low-pass filtered IF signal is then given as

$$\begin{aligned} y_O(t) &= [A_O\, s(t)\, s(t-\tau_O) + v_2(t)] * h_L(t) \\ &= \frac{A^2 A_O}{2}\cos\left(2\pi f_{BO} t + \Phi_O + \varphi(t) - \varphi(t-\tau_O)\right) \\ &\quad + v_{2L}(t), \end{aligned} \tag{8}$$

with $f_{BO} = k\tau_O$ and $\Phi_O = 2\pi f_0 \tau_O - k\pi\tau_O^2$. Equivalently to $v_1(t)$, the intrinsic noise is modeled as a white Gaussian noise process, contributing to the OCT IF signal as $v_{2L}(t) = v_2(t) * h_L(t)$.

Note that the architecture of the OCT is similar to the well-known *delay line discriminator* (DLD) method [14] often utilized for on-chip phase noise measurement. It requires a delay line and a phase shifter to obtain the PN of the oscillator under test. However, in contrast to the DLD method the OCT is fed by a linear frequency modulated signal, i.e., $s(t)$. This way the phase shifter is no longer capable to generate the required constant 90° phase shift between the LO and RF inputs of the mixer. Even more important, it will be shown later that the proposed SR leakage cancelation concept uses the instantaneous DPN, and hence, as in [15] no phase shifter is required.

By comparing (4) and (8) it is easily verified that choosing $\tau_O = \tau_S$ and $A_O = A'_S$ would theoretically allow ideal SR leakage cancelation with the OCT. However, there is a tough limitation of delay lines realized within MMICs. These delay lines can be built with transmission lines, passive LC filters or inverter structures [16], [17]. For the latter only bipolar transistors are applicable, as CMOS transistors have transit frequencies of some GHz only.

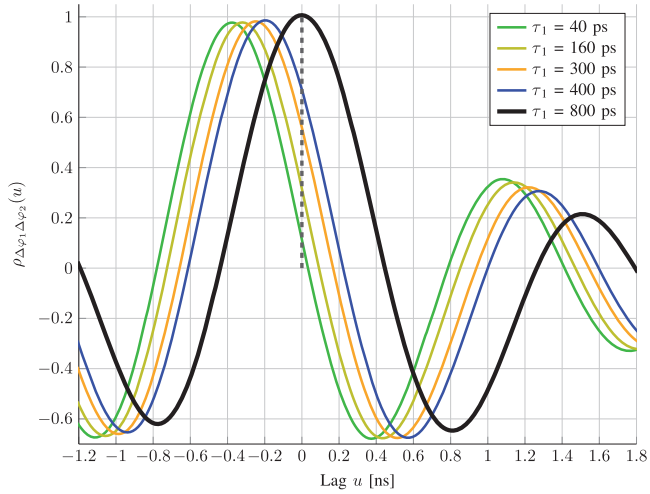

Fig. 5. Approximation of the normalized cross-covariance $\rho_{\Delta\varphi_1\Delta\varphi_2}(u)$ for a fixed $\tau_2 = 800$ ps and τ_1 varied in the range of 40 to 800 ps. It is evaluated in a discrete-time simulation, where the expectation operator is approximated over a statistically representative number of samples.

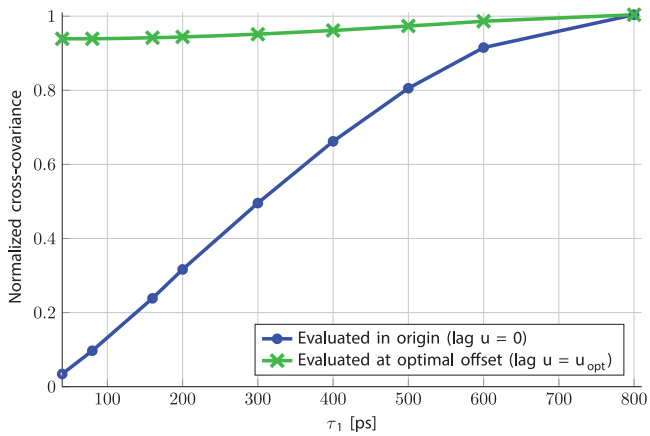

Fig. 6. Normalized cross-covariance evaluated in the origin ($u = 0$) and at the optimum lag u_{opt}. The latter shows a severely better correlation between the two DPNs $\Delta\varphi_1$ and $\Delta\varphi_2$.

Assuming the RTDT of the SR leakage to be in the range of a nanosecond, an on-chip delay that achieves this amount of delay would increase the chip area significantly. This makes the concept proposed in [10] unfeasible to solve the problem at hand. We therefore aim to perform leakage cancelation with the constraint that τ_O is significantly smaller than τ_S.

III. Cross-Correlation Properties of Decorrelated Phase Noise

In Section II-D it was shown that the DPN of the SR leakage increases the system noise floor such that the target detection sensitivity is deteriorated. Given the constraint that the delay τ_O of the OCT is significantly smaller than the RTDT τ_S of the SR leakage, we now investigate the DPN in time domain and the cross-correlation properties between two respective DPN terms.

A. Decorrelated Phase Noise in Time Domain

We depart from the FMCW radar system model in this Section and solely analyze the DPN. For a delay τ_1 the DPN is given as

$$\Delta\varphi_1(t) = \varphi(t) - \varphi(t-\tau_1). \tag{9}$$

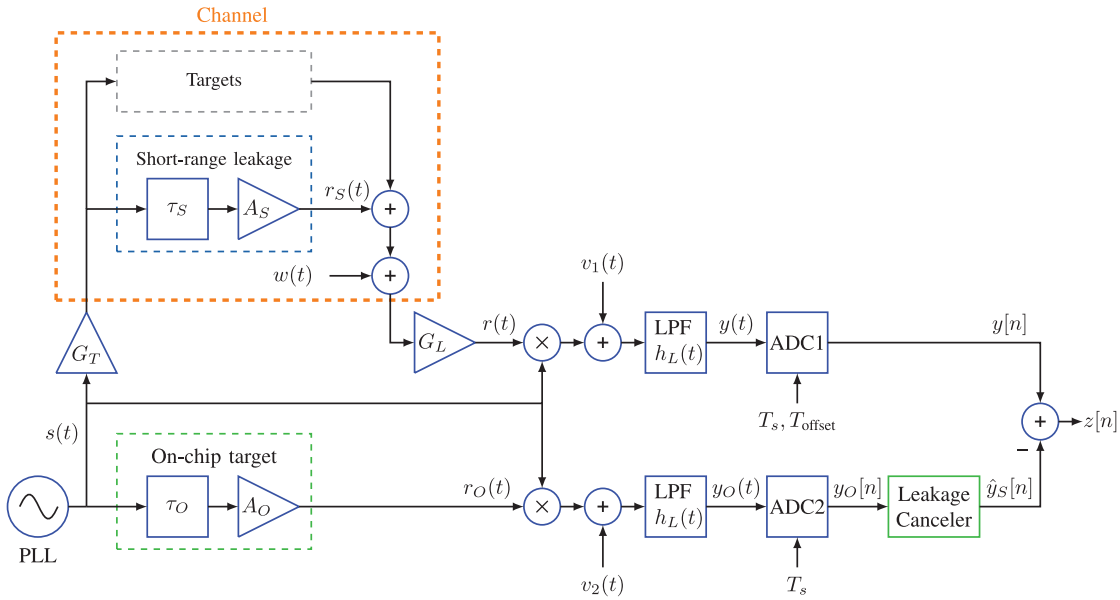

Fig. 7. System model with the artificial on-chip target. As the channel, it is fed by the same chirp signal from the PLL and its output signal $r_O(t)$ is downconverted with the instantaneous transmit signal $s(t)$. The essential difference to the channel reflections is that the OCT signal isn't perturbed by other reflections or the AWGN $w(t)$ but is limited only by the intrinsic noise. The leakage canceler can thus extract the DPN from the OCT IF signal and generate the cancelation signal $\hat{y}_S[n]$.

The PN $\varphi(t)$ is considered as a stationary random process. For simulation purposes it is generated from white Gaussian noise sent through an LTI system. It is specified by the power spectrum $S_{\varphi\varphi}(f)$. Fig. 3 depicts $\Delta\varphi_1(t)$ according to (9) for different delays τ_1 in the range of $40 \ldots 800$ ps and a realization of the PN $\varphi(t)$ with the exemplary power spectrum as given in Fig. 2. There is a noticeable similarity between the array of curves, that is they are more or less shifted in time and scaled in amplitude. The latter is due to the range correlation effect, which can be observed in Fig. 3 directly in the time-domain. The smaller the delay τ_1, the smaller becomes the DPN's amplitude.

B. Cross-Correlation Properties

In order to compare DPN terms with different delays we employ a simple model as given in Fig. 4. We therefore introduce a second delay τ_2, for which we assume that $\tau_1 \leq \tau_2$. Analogous to (9) we define its DPN

$$\Delta\varphi_2(t) = \varphi(t) - \varphi(t - \tau_2). \tag{10}$$

To quantify the similarity observed from the array of curves in Fig. 3, we employ the cross-covariance function between $\Delta\varphi_1(t)$ and $\Delta\varphi_2(t)$. With the stationarity assumption and the fact that the DPN terms have zero mean it is given as

$$c_{\Delta\varphi_1\Delta\varphi_2}(u) = \mathrm{E}\{\Delta\varphi_1(t)\Delta\varphi_2(t+u)\}, \tag{11}$$

where u is the time lag and $\mathrm{E}\{\cdot\}$ is the expectation operator. Note that since the DPN has zero mean, the cross-covariance equals the cross-correlation.

Further, the normalized cross-covariance between $\Delta\varphi_1$ and $\Delta\varphi_2$ is given as

$$\rho_{\Delta\varphi_1\Delta\varphi_2}(u) = \frac{c_{\Delta\varphi_1\Delta\varphi_2}(u)}{\sqrt{\sigma^2_{\Delta\varphi_1}\sigma^2_{\Delta\varphi_2}}}, \tag{12}$$

where $\sigma^2_{\Delta\varphi_1}$ and $\sigma^2_{\Delta\varphi_2}$ are the variances of the two DPN processes, respectively. A numerical approximation of the normalized cross-covariance $\rho_{\Delta\varphi_1\Delta\varphi_2}(u)$ is depicted in Fig. 5 for a fixed $\tau_2 = 800$ ps and τ_1 varied in the range of 40 to 800 ps. It was evaluated in a discrete-time simulation, where the expectation operator was approximated over a statistically representative number of samples. It is clear that with $\tau_1 = \tau_2$ we achieve perfect correlation such that the normalized cross-covariance evaluated at zero lag becomes $\rho_{\Delta\varphi_1\Delta\varphi_2}(0)|_{\tau_1=\tau_2} = 1$.

With decreasing delay τ_1 the normalized cross-covariance steeply decays when evaluated at $\rho_{\Delta\varphi_1\Delta\varphi_2}(0)$ (dashed line in Fig. 5). However, the maxima of each of the normalized cross-covariances are shifted towards a negative lag with decreasing τ_1, or an increasing difference $\tau_2 - \tau_1$. Note that the same time shift was already observed in Fig. 3. To compensate for this shift we derive the optimum lag subsequently.

C. Optimum Lag

The optimum lag u that maximizes the normalized cross-covariance depends on the delays τ_1 and τ_2 ($\tau_1 < \tau_2$). To derive this optimum lag we utilize the cross-covariance function as given in (11). Substituting the DPNs with (9) and (10) gives

$$\begin{aligned} c_{\Delta\varphi_1\Delta\varphi_2}(u) = \mathrm{E}\{&[\varphi(t) - \varphi(t-\tau_1)] \\ &[\varphi(t+u) - \varphi(t+u-\tau_2)]\} \\ = \mathrm{E}\{&\varphi(t)\,\varphi(t+u) \\ &- \varphi(t)\,\varphi(t+u-\tau_2) \\ &- \varphi(t-\tau_1)\,\varphi(t+u) \\ &+ \varphi(t-\tau_1)\,\varphi(t+u-\tau_2)\}. \end{aligned} \tag{13}$$

Note that the resulting equation merely consists of auto-covariance functions. Introducing it for the zero mean PN as

$$c_{\varphi\varphi}(u) = \mathrm{E}\{\varphi(t)\varphi(t+u)\}, \tag{14}$$

Equation (13) can be rewritten as

$$c_{\Delta\varphi_1\Delta\varphi_2}(u) = c_{\varphi\varphi}(u) - c_{\varphi\varphi}(l-\tau_2) - c_{\varphi\varphi}(l+\tau_1) + c_{\varphi\varphi}(l-\tau_2+\tau_1). \quad (15)$$

Utilizing the *Wiener-Khintchine-Theorem*

$$c_{\varphi\varphi}(u) = \int_{-\infty}^{\infty} S_{\varphi\varphi}(f) e^{j2\pi u f}\, df, \quad (16)$$

we are able to compute the auto-covariance function, which equals the auto-correlation function of the PN as it has zero mean. The shape of $c_{\varphi\varphi}(u)$ is therefore defined by the power spectrum $S_{\varphi\varphi}(f)$. For the optimization problem at hand we approximate $c_{\varphi\varphi}(u)$ as 4th order polynomial in the range of $-\tau_2+\tau_1 \leq u \leq 0$. Applying this approximation to (15), differentiating it w.r.t. u, setting the result to zero and solving for u reveals the optimum lag that maximizes (11) depending on the delays τ_1 and τ_2 as

$$u_{\text{opt}} = -\frac{\tau_2-\tau_1}{2} \quad (17)$$

for the exemplary PN power spectrum $S_{\varphi\varphi}(f)$ depicted in Fig. 2.

The numerical approximation of the normalized cross-covariance $\rho_{\Delta\varphi_1\Delta\varphi_2}(u)$ evaluated in the origin, that is $u=0$, against $\rho_{\Delta\varphi_1\Delta\varphi_2}(u)$ evaluated at the optimum lag u_{opt} is depicted in Fig. 6. For the former case the values of the normalized cross-covariance decay fast with τ_1 becoming smaller. However, evaluating $\rho_{\Delta\varphi_1\Delta\varphi_2}(u)$ at the optimum lags u_{opt} results in significantly higher values. This suggests that $\Delta\varphi_2(t)$ can be estimated from a shifted version of $\Delta\varphi_1(t)$. Note that the correlation is present up to very large τ_2/τ_1 ratios. For instance, with $\tau_2 = 800$ ps and $\tau_1 = 40$ ps, that is a τ_2/τ_1 ratio of 20, we still obtain a normalized cross-covariance of 0.94.

D. Linear MMSE Prediction of $\Delta\varphi_2(t)$

In order to estimate the instantaneous DPN $\Delta\varphi_2(t)$ from $\Delta\varphi_1(t)$ we use a linear predictor. With the two DPNs having zero mean, the best linear estimator in the minimum mean square error (MMSE) sense is given as [18]

$$\hat{\Delta\varphi_2}(t+u_{\text{opt}}) = \frac{c_{\Delta\varphi_1\Delta\varphi_2}(u_{\text{opt}})}{c_{\Delta\varphi_1\Delta\varphi_1}(0)}\Delta\varphi_1(t), \quad (18)$$

where we introduce the DPN scaling factor as

$$\alpha = \frac{c_{\Delta\varphi_1\Delta\varphi_2}(u_{\text{opt}})}{c_{\Delta\varphi_1\Delta\varphi_1}(0)}. \quad (19)$$

Note that the optimum lag u_{opt} is incorporated into the estimator in (18).

E. Scaling Factor With Lowpass Filtered DPN

So far the PN has been considered as stationary random process with PSD $S_{\varphi\varphi}(f)$, which causes the DPN to have infinite bandwidth. However, in the FMCW radar system model introduced in Section II the DPN becomes lowpass filtered. This filtering with impulse response $h_L(t)$ is crucial for the computation of the DPN scaling factor.

The lowpass filtered versions of the two DPN terms are given as

$$\Delta\varphi_{1L}(t) = \Delta\varphi_1(t) * h_L(t), \quad (20)$$
$$\Delta\varphi_{2L}(t) = \Delta\varphi_2(t) * h_L(t) \quad (21)$$

such that the DPN scaling factor from (19) incorporating the filtering process becomes

$$\begin{aligned}\alpha_L &= \frac{c_{\Delta\varphi_{1L}\Delta\varphi_{2L}}(u_{\text{opt}})}{c_{\Delta\varphi_{1L}\Delta\varphi_{1L}}(0)} \\ &= \frac{\mathrm{E}\{\Delta\varphi_{1L}(t)\,\Delta\varphi_{2L}(t+u\text{opt})\}}{\mathrm{E}\{\Delta\varphi_{1L}(t)\,\Delta\varphi_{1L}(t)\}} \\ &= \frac{\mathrm{E}\{[\Delta\varphi_1(t)*h_L(t)]\;[\Delta\varphi_2(t+u_{\text{opt}})*h_L(t)]\}}{\mathrm{E}\{[\Delta\varphi_1(t)*h_L(t)]\;[\Delta\varphi_1(t)*h_L(t)]\}}.\end{aligned} \quad (22)$$

From the equation above it can be seen that α_L is computed from the filtered versions of the auto- and cross-covariance functions of the DPN terms $\Delta\varphi_1(t)$ and $\Delta\varphi_2(t)$, respectively. With the *Wiener-Lee* identity we have that

$$c_{\Delta\varphi_{1L}\Delta\varphi_{1L}}(u) = c_{\Delta\varphi_1\Delta\varphi_1}(u) * c^E_{h_Lh_L}(u), \quad (23)$$

where $c^E_{h_Lh_L}(u)$ is the energy ACF of the impulse response $h_L(t)$ of the lowpass filter. It can be shown that the *Wiener-Lee* identity also holds for the cross-covariance such that

$$c_{\Delta\varphi_{1L}\Delta\varphi_{2L}}(u) = c_{\Delta\varphi_1\Delta\varphi_2}(u) * c^E_{h_Lh_L}(u). \quad (24)$$

With this result we can also write the Fourier transforms of (23) and (24) in similar and compact forms, that is

$$S_{\Delta\varphi_{1L}\Delta\varphi_{1L}}(f) = S_{\Delta\varphi_1\Delta\varphi_1}(f)\,|H_L(f)|^2, \quad (25)$$
$$S_{\Delta\varphi_{1L}\Delta\varphi_{2L}}(f) = S_{\Delta\varphi_1\Delta\varphi_2}(f)\,|H_L(f)|^2. \quad (26)$$

However, for an analytical description of $S_{\Delta\varphi_{1L}\Delta\varphi_{1L}}(f)$ and $S_{\Delta\varphi_{1L}\Delta\varphi_{2L}}(f)$ it is desirable to express them in terms of $S_{\varphi\varphi}(f)$ as this PSD is well known from the design specifications of the frequency generating circuit. From the range correlation effect [9] we know that

$$S_{\Delta\varphi_1\Delta\varphi_1}(f) = S_{\varphi\varphi}(f)\,\kappa_{\tau_1}(f) \quad (27)$$

with $\kappa_{\tau_1} = 2\,(1-\cos(2\pi f\tau_1))$. To determine the cross PSD we express (13) as

$$c_{\Delta\varphi_1\Delta\varphi_2}(u) = c_{\varphi\varphi}(u) - c_{\varphi\varphi}(u-\tau_2) - c_{\varphi\varphi}(u+\tau_1) + c_{\varphi\varphi}(u+\tau_1-\tau_2), \quad (28)$$

and therewith its PSD is, according to the *Wiener-Khinchine* theorem, given as

$$\begin{aligned}S_{\Delta\varphi_1\Delta\varphi_2}(f) &= S_{\varphi\varphi}(f) - S_{\varphi\varphi}(f)\,e^{j2\pi f\tau_2} \\ &\quad - S_{\varphi\varphi}(f)\,e^{-j2\pi f\tau_1} + S_{\varphi\varphi}(f)\,e^{-j2\pi f(\tau_1-\tau_2)} \\ &= S_{\varphi\varphi}(f)\,\kappa_{\tau_1\tau_2}(f)\end{aligned} \quad (29)$$

with $\kappa_{\tau_1\tau_2}(f) = 1 - e^{j2\pi f\tau_2} - e^{-j2\pi f\tau_1} + e^{-j2\pi f(\tau_1-\tau_2)}$.

TABLE I
EXEMPLARY VALUES FOR THE DPN SCALING FACTORS α AND α_L WITH DIFFERENT τ_2/τ_1 RATIOS.

τ_1 [ps]	τ_2 [ps]	τ_2/τ_1 ratio	u_{opt} [ps]	DPN scaling factor α	DPN scaling factor α_L
40	800	20	-380	11.76	19.974
80	800	10	-360	6.45	9.987
160	800	5	-320	3.28	4.993
400	800	2	-200	1.43	1.995

Plugging in (27) and (29) the lowpass filtered PSDs from (25) and (26) become

$$S_{\Delta\varphi_{1L}\Delta\varphi_{1L}}(f) = S_{\varphi\varphi}(f)\,\kappa_{\tau_1}(f)\,|H_L(f)|^2,$$
$$S_{\Delta\varphi_{1L}\Delta\varphi_{2L}}(f) = S_{\varphi\varphi}(f)\,\kappa_{\tau_1\tau_2}(f)\,|H_L(f)|^2. \quad (30)$$

Finally, with the inverse *Wiener-Khinchine* theorem the DPN scaling factor from (22) becomes

$$\alpha_L = \frac{\int_{-\infty}^{\infty} S_{\Delta\varphi_{1L}\Delta\varphi_{2L}}(f) e^{j2\pi f u_{\text{opt}}} df}{\int_{-\infty}^{\infty} S_{\Delta\varphi_{1L}\Delta\varphi_{1L}}(f) e^{j2\pi f 0} df} = \frac{\int_{-\infty}^{\infty} S_{\varphi\varphi}(f)\,\kappa_{\tau_1\tau_2}(f)\,|H_L(f)|^2\, e^{j2\pi f u_{\text{opt}}}\, df}{\int_{-\infty}^{\infty} S_{\varphi\varphi}(f)\,\kappa_{\tau_1}(f)\,|H_L(f)|^2\, df}. \quad (31)$$

Note that the computation of α_L merely requires knowledge of the delays τ_1, τ_2, the PN PSD $S_{\varphi\varphi}(f)$ and the filter characteristics.

For completeness, numerical approximations of α and α_L are given in Table I for different τ_2/τ_1 ratios. For that an ideal lowpass filter with a cutoff frequency of $f_c = 25$ MHz and the exemplary PN power spectrum $S_{\varphi\varphi}(f)$ from Fig. 2 are assumed. As can be seen from Table I, α_L is larger than α for all τ_2/τ_1 ratios.

In conclusion, α and α_L are measures of how much the DPNs $\Delta\varphi_1(t)$ and $\Delta\varphi_{1L}(t)$, respectively, need to be scaled such that they approximate $\Delta\varphi_2$ and $\Delta\varphi_{2L}(t)$ well. This finding will be applied in the next section to estimate the DPN of the SR leakage with that of the OCT.

IV. SHORT-RANGE LEAKAGE CANCELATION

A. Cross-Correlation Properties Applied to the FMCW Radar System Model

In the previous section it was shown that there is a noticeable correlation between the two DPN terms for different delays τ_1 and τ_2. For the problem at hand the DPN of the artificial on-chip target (delay τ_O) and the SR leakage (delay τ_S) are at stake, where due to circuit design limitations we constrain $\tau_O < \tau_S$. This constraint has also been assumed in Section III ($\tau_1 < \tau_2$). Also, the delays considered for τ_1 and τ_2 were assumed below one nanosecond. This equals a radar target distance of up to 15 cm, which is the approximate range of the SR target distance. Consequently, with the findings from the previous section we are now able to propose the actual SR leakage cancelation algorithm, to be carried out in the digital IF domain.

The on-chip target is integrated into the system model as depicted in Fig. 7. In parallel to the channel, it is fed by the same transmit signal $s(t)$. Further, downconversion to the IF and subsequent lowpass filtering is done.

With regard to the system model at hand, the optimum lag u_{opt} that was derived in Section III-C, is realized in the FMCW radar system model by slightly delaying the sampling clock of the ADC of the upper signal path (channel). This is indicated by T_{offset} in Fig. 7. According to (17) the optimum sampling clock offset is

$$T_{\text{offset}} = -\frac{\tau_S - \tau_O}{2}. \quad (32)$$

Given the physical constraints for τ_S and τ_O, the sampling clock offset T_{offset} will be in the range of some hundred picoseconds. Assuming the ADC sampling frequency to be in the MHz range, T_{offset} is only a fraction of the sampling interval T_s.

The DPN scaling factor α_L can be computed readily from (31) as

$$\alpha_L = \frac{\int_{-\infty}^{\infty} S_{\varphi\varphi}(f)\,\kappa_{\tau_O\tau_S}(f)\,|H_L(f)|^2\, e^{j2\pi f T_{\text{offset}}}\, df}{\int_{-\infty}^{\infty} S_{\varphi\varphi}(f)\,\kappa_{\tau_O}(f)\,|H_L(f)|^2\, df} \quad (33)$$

and the linear MMSE prediction of the DPN of the SR leakage follows to

$$\hat{\Delta\varphi}_S(t + T_{\text{offset}}) = \alpha_L\,\Delta\varphi_O(t). \quad (34)$$

Considering the FMCW radar system model all the parameters in (32) and (33) except τ_S are well known design parameters. However, since for a specific application scenario τ_S can be tightly constrained, an offline computation of the DPN scaling factor is feasible. In case τ_S changes slightly over time, a look up table could be used to readjust α_L in a regular manner.

The aim of the leakage canceler introduced in Fig. 7 is to find the cancelation signal $\hat{y}_S[n]$ given $y_O[n]$, where the latter is the discrete-time version of $y_O(t)$ with time index n. Since τ_O is smaller than τ_S, the resulting beat frequencies and the constant phase offsets in their respective IF signals are different. The leakage canceler therefore has to employ the following steps:

1) Extract the DPN from the OCT IF signal with beat frequency f_{BO} (Section IV-B).
2) Generate the expected sinusoidal corresponding to the SR leakage with beat frequency f_{BS} including DPN from step 1 to obtain $\hat{y}_S[n]$ and subtract it from the receive signal $y[n]$ (Section IV-C).

These steps are carried out in detail in the next two subsections.

B. Decorrelated Phase Noise Extraction From the OCT IF Signal

Since the leakage cancelation is performed in the digital IF domain, we sample (8) with sampling frequency f_s, which gives

$$y_O[n] = \frac{A^2 A_O}{2}\cos\left(2\pi f_{BO} n T_s + \Phi_O + \Delta\varphi_O[n]\right) + v_{2L}[nT_s], \quad (35)$$

where $T_s = 1/f_s$ is the sampling interval. We aim to extract the DPN term, whose sampled version is given as $\Delta\varphi_O[n] = \varphi(nT_s) - \varphi(nT_s - \tau_O)$, that is we obtain the difference between the two instantaneous phase noise values at time step n. As done for the SR leakage, we now apply the cosine sum

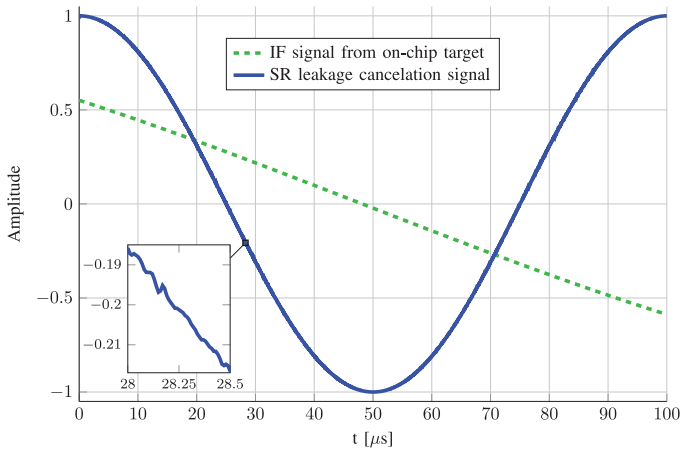

Fig. 8. OCT IF signal $y_O[n]$ and SR leakage cancelation signal $\hat{y}_S[n]$ over a single chirp with $\tau_S/\tau_O = 5$. In the zoom window the DPN incorporated into the SR leakage cancelation signal $\hat{y}_S[n]$ becomes visible. The IF signals are normalized to have unit amplitude.

identity to (35), such that, together with $\cos(\Delta\varphi_O[n]) \approx 1$ and $\sin(\Delta\varphi_O[n]) \approx \Delta\varphi_O[n]$, it can be approximated as

$$y_O[n] \approx \frac{A^2 A_O}{2}\cos(2\pi f_{BO} n T_s + \Phi_O) - \frac{A^2 A_O}{2}\sin(2\pi f_{BO} n T_s + \Phi_O)\,\Delta\varphi_O[n] + v_{2L}[nT_s]. \quad (36)$$

Hence, we can extract the DPN as

$$\Delta\varphi_O[n] \approx \frac{\frac{A^2 A_O}{2}\cos(2\pi f_{BO} n T_s + \Phi_O) - y_O[n] + v_{2L}[nT_s]}{\frac{A^2 A_O}{2}\sin(2\pi f_{BO} n T_s + \Phi_O)} \quad (37)$$

Since the circuit design parameters τ_O and A_O are well known, the OCT beat frequency and the constant phase can be determined as $f_{BO} = (B/T)\tau_O$ and $\Phi_O = 2\pi f_0 \tau_O - k\pi\tau_O^2$, respectively.

C. Generation of the SR Leakage Cancelation Signal

In Section III it was shown that the DPN $\Delta\varphi_O[n]$ is highly correlated to $\Delta\varphi_S[n]$ for a τ_S/τ_O ratio of up to 20. This finding is now utilized to generate the cancelation signal $\hat{y}_S[n]$.

Based on (4) we define the cancelation signal as

$$\hat{y}_S[n] = \frac{A^2 \hat{A}'_S}{2}\cos(2\pi \hat{f}_{BS} n T_s + \hat{\Phi}_S + \alpha_L\,\Delta\varphi_O[n]), \quad (38)$$

where $\hat{A}'_S = G_T \hat{A}_S G_L$ is the expected SR leakage reflection gain, $\hat{f}_{BS}$ is the expected beat frequency, $\hat{\Phi}_S$ is the expected phase and α_L is the DPN scaling factor derived in Section III-E. The OCT IF signal $y_O[n]$ and the SR leakage cancelation signal $\hat{y}_S[n]$ are compared in Fig. 8. It can be observed that the beat frequency of the SR leakage IF signal is τ_S/τ_O times larger than that of the OCT IF signal. Further, the zoom window in Fig. 8 depicts the SR leakage cancelation signal $\hat{y}_S[n]$ in more detail. Therein, the incorporated DPN from the OCT becomes visible.

Clearly, the parameters τ_S and A'_S cannot be estimated as precise as those of the OCT as the SR leakage reflections are superimposed by the channel reflections and the AWGN. Still they can be constrained tightly given a certain hardware setup of the radar device. This might be done as part of a regular calibration process. As the SR leakage is superimposed by other reflections, it is desirable to perform this calibration when there are no targets in the channel at all. Note that since the leakage canceler is implemented in digital hardware, a changing environment can be tracked in an adaptive manner.

The final step is simply to subtract the expected SR leakage signal from the received signal, that is

$$z[n] = y[n] - \hat{y}_S[n]. \quad (39)$$

D. Limitations of DPN Extraction

In Section IV-B it was shown that the DPN can be extracted from the OCT in the digital IF domain. However, according to the range correlation effect the DPN power decreases with τ_O. Hence, a minimum on-chip delay is required such that the DPN power exceeds that of the intrinsic noise $v_2(t)$. We provide a detailed investigation on this requirement in [17]. Therein we show that the optimum OCT delay is $\tau_O = 192$ ps for the same system parameters as used in this paper.

Furthermore, as the leakage cancelation is employed in the digital domain, also the quantization noise must remain well below the DPN signal power of the OCT given as [17]

$$P_{\Delta\varphi_O} = \int_{-f_c}^{f_c} 2\,S_{\varphi\varphi}(f)\,(1 - \cos(2\pi f \tau_O))\,df. \quad (40)$$

For an ideal ADC we have that the signal to quantization noise ratio (SQNR) for sinusoidal signals is

$$\text{SQNR} \approx 1.76\text{ dB} + 20\log_{10}(2^Q), \quad (41)$$

where Q is the resolution of the ADC.

To compute the required resolution for the problem at hand, we exemplarily consider a PLL output power of 0 dBm, an on-chip delay line with $\tau_O = 192$ ps and $A_O = -6$ dB insertion loss, and a passive mixer with -7 dB conversion loss. Further, we assume an ADC with a full scale input power of 0 dBm and a proper preamplifier with 12 dB gain that scales $y_O(t)$ to have -1 dBm, i.e., a 1 dB margin to the full scale range. The sampling frequency is $f_s = 100$ MHz and the lowpass filter cutoff frequency is $f_c = 50$ MHz. The resulting integrated DPN power is $P_{\Delta\varphi_O} = -77.2$ dBm in the Nyquist bandwidth. Thus, an ADC with at least 13 bits resolution is required that delivers an SQNR of 80.0 dB.

E. MIMO Scenario

In order to measure not only the distance but also the angular position of targets, multiple-input multiple-output (MIMO) radars are utilized [19]. The angle is estimated out of the different round-trip delay times from the transmit to the receive antennas. Consequently, the beat frequencies and phase terms in the IF domain differ for each of the receive paths. That is, for cancelation of the SR leakage, the parameters of the sinusoidal waves need to be adjusted to all these paths. However, due to the DPN cross-correlation properties shown in Section III, only a single OCT is required to estimate the DPN and apply it to the expected SR leakage IF signals.

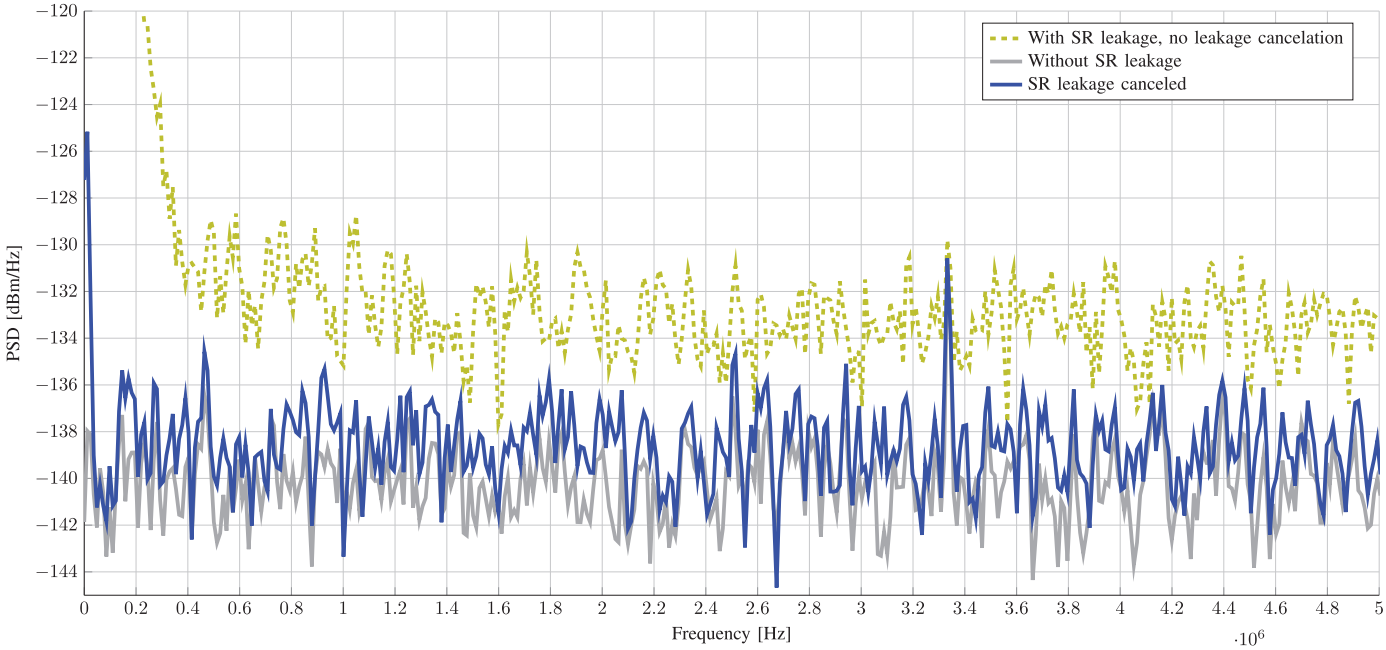

Fig. 9. Hann-windowed power spectrum estimation of the IF signals for different scenarios, averaged over 8 chirps. The system simulated with SR leakage but without its cancelation results in a noise floor that is dominated by the DPN. Without SR leakage present at all the AWGN sets the systems noise floor and therewith the target detection sensitivity. With the proposed SR leakage cancelation in place the DPN of the SR leakage is significantly suppressed and therewith the target with a beat frequency of around 3.33 MHz is resolved well.

F. Realization Within an MMIC

The hardware requirements for the proposed SR leakage cancelation concept regarding analog circuitry are the on-chip delay line, the mixer, the lowpass filter and the ADC. Any further signal processing is done in the digital IF domain, such that compared to [2], [4] no further modulators or couplers are required. The delay line of the OCT can be realized with a passive LC filter with low insertion loss [20], thus also a passive mixer can be instantiated for the OCT path. This is beneficial as the intrinsic noise $v_2(t)$ is then defined by the thermal noise.

In the digital domain the extraction of the DPN $\Delta\varphi_O[n]$ as well as generation of the SR leakage cancelation signal $\hat{y}_S[n]$ can be performed online. That is, only instantaneous samples from ADC2 are utilized and as a result the algorithm requires a negligible amount of memory.

As discussed in Section IV-E the proposed concept for SR leakage cancelation is applicable also for MIMO systems. Therefore, no additional analog circuitry is required as a single OCT is sufficient for estimation of the DPN.

V. Simulation Results

In this section a full FMCW radar system simulation is carried out to show the effectiveness of the proposed leakage cancelation algorithm. The simulation environment is based on Fig. 7. The system parameters are chosen according to a typical automotive radar system.

For the sake of a fast simulation the FMCW chirp start frequency is set to $f_0 = 6$ GHz, instead of the typically used 76 GHz for automotive applications. However, the proposed concept works in the same way for higher carrier frequencies as the essential signal processing is done in the IF domain. The sweep bandwidth is chosen to be $B = 1$ GHz which is ramped within $T = 100$ μs. The PLL output signal power is 0 dBm, while the transmit power amplifier and the receive LNA have a gain of $G_T = 10$ dB and $G_L = 20$ dB, respectively.

The channel comprises of the SR leakage with an RTDT $\tau_S = 1$ ns (distance $d_S \approx 15$ cm), $A_S = -8$ dB and a single target with $\tau_{T1} = 333$ ns (distance $d_{T1} \approx 50$ m). The OCT parameters are chosen as $\tau_O = 192$ ps (resulting d_S/d_O ratio is approximately 5) and $A_O = -6$ dB. For the OCT path a passive mixer with a conversion loss of -7 dB is used.

The AWGN $w_L(t)$ from the channel and the intrinsic noise $v_{1L}(t)$ are assumed to have a total noise floor at $S_{w_L w_L}(f) + S_{v_{1L} v_{1L}}(f) = -140$ dBm/Hz in the IF domain. The intrinsic noise of the OCT path $v_{2L}(t)$ will be varied for comparison. The noise sources $w(t)$, $v_1(t)$ and $v_2(t)$ are white Gaussian noise processes and assumed to be uncorrelated.

Considering the sampling frequency of the ADC to be $f_s = 100$ MHz, we choose the cutoff frequencies of the lowpass filters as $f_c = 25$ MHz. They are modeled as 6th order infinite impulse response Butterworth filters. The ADC sampling offset T_{offset} and the DPN scaling factor α_L are computed according to (32) and (33). The ADC is simulated with a resolution of 15 bits. Further, the lowpass filtered OCT IF signal is pre-amplified such that the ADC is operated in full range.

The resulting beat frequencies for the OCT and SR leakage are $f_{BO} = 666$ Hz and $f_{BS} = 6.67$ kHz, respectively. The IF PSD averaged over 8 chirps is given in Fig. 9 for different scenarios.

Firstly, with SR leakage but no leakage cancelation a peak close to DC originated from the beat frequency f_{BS} occurs. The overall system's noise floor is increased as has been observed analytically already in Section II-D. Consequently the target T_1 with a beat frequency of around 3.33 MHz is covered in noise.

Secondly, assuming that no SR leakage is present in the system, the AWGN sets the noise floor. Therewith, the target T_1 is resolved well.

Thirdly, with SR leakage and the proposed cancelation algorithm with the OCT in place. The OCT signal path is simulated with an intrinsic noise floor of $S_{v_{2L}v_{2L}}(f) = -174$ dBm/Hz, that is the thermal noise floor since the OCT comprises of passive circuitry only. It can be seen in Fig. 9 that the effect of the DPN from the SR leakage is suppressed by 6.4 dB and that the target T_1 is resolved well. For comparison, choosing $S_{v_{2L}v_{2L}}(f) = -170$ dBm/Hz leads to a suppression of 4.5 dB. This evidences the effectiveness of the proposed method. Still, the intrinsic noise is crucial for the cancelation performance. To increase the margin from the DPN power to the intrinsic noise, several OCTs could be placed in parallel and its outputs summed.

VI. Conclusion

The short-range leakage, which models a disturbing reflection from an object right in front of the antennas, permanently superimposes the actual target reflections due to the continuous operation of the FMCW radar. To mitigate the SR leakage an artificial on-chip target, essentially consisting of a delay line, was introduced. The obvious approach for the delay of the OCT would be to mimic the round-trip delay time of the SR target, and to subtract the OCTs output signal from the actual receive signal. However, a practically useful delay in this range cannot be integrated into an MMIC. It turns out that a significantly smaller delay suffices to obtain a good estimate of the DPN, which was proven analytically by correlation statistics. This suggests the integration of the OCT in MMICs. Since the actual leakage cancelation is done in the digital IF domain, the concept is applicable to FMCW radar transceivers with arbitrary carrier frequencies. Furthermore, the leakage canceler can be easily reconfigured for different hardware setups.

Acknowledgment

The authors thank R. Stuhlberger for his most valuable inputs.

References

[1] C. Wagner, A. Stelzer, and H. Jäger, "Adaptive frequency sweep linearization based on phase accumulator principle," in *Proc. IEEE/MTT-S Int. Microw. Symp.*, Jun. 2007, pp. 1319–1322.

[2] K. Lin, Y. Wang, C. Pao, and Y. Shih, "A Ka-band FMCW radar front-end with adaptive leakage cancellation," *IEEE Trans. Microw. Theory Tech.*, vol. 54, no. 12, pp. 4041–4048, Dec. 2006.

[3] A. G. Stove, "Linear FMCW radar techniques," *IEE Proc. F, Radar Signal Process.*, vol. 139, no. 5, pp. 343–350, Oct. 1992.

[4] K. Lin and Y. Wang, "Transmitter noise cancellation in monostatic FMCW radar," in *IEEE/MTT-S Int. Microw. Symp. Dig.*, Jun. 2006, pp. 1406–1409.

[5] R. Feger, C. Wagner, and A. Stelzer, "An IQ-modulator based heterodyne 77-GHz FMCW radar," in *Proc. German Microw. Conf. (GeMIC)*, Mar. 2011, pp. 1–4.

[6] J. Lee *et al.*, "A UHF mobile RFID reader IC with self-leakage canceller," in *Proc. Radio Freq. Integr. Circuits Symp. (RFIC)*, Honolulu, HI, USA, Jun. 2007, pp. 273–276.

[7] C. Lederer and M. Huemer, "LMS based digital cancellation of second-order TX intermodulation products in homodyne receivers," in *Proc. Radio Wireless Symp. (RWS)*, Phoenix, AZ, USA, Jan. 2011, pp. 207–210.

[8] C. Lederer and M. Huemer, "Simplified complex LMS algorithm for the cancellation of second-order TX intermodulation distortions in homodyne receivers," in *Conf.. Rec. 45th Asilomar Conf. Signals, Syst., Comput. (ASILOMAR)*, Pacific Grove, CA, USA, Nov. 2011, pp. 533–537.

[9] M. C. Budge Jr. and M. P. Burt, "Range correlation effects in radars," in *Rec. IEEE Nat. Radar Conf.*, Lynnfield, MA, USA, 1993, pp. 212–216.

[10] M. A. Gonzalez, J. Grajal, A. Asensio, D. Madueno, and L. Requejo, "A detailed study and implementation of an RPC for LFM-CW radar," in *Proc. 36th Eur. Microw. Conf.*, Manchester, U.K., Sep. 2006, pp. 1806–1809.

[11] M. Vossiek, P. Heide, M. Nalezinski, and V. Magori, "Novel FMCW radar system concept with adaptive compensation of phase errors," in *Proc. 26th Eur. Microw. Conf.*, Prague, Czech Republic, Sep. 1996, pp. 135–139.

[12] L. Reindl, C. C. W. Ruppel, S. Berek, U. Knauer, M. Vossiek, P. Heide, and L. Oreans, "Design, fabrication, and application of precise SAW delay lines used in an FMCW radar system," *IEEE Trans. Microw. Theory Tech.*, vol. 49, no. 4, pp. 787–794, Apr. 2001.

[13] A. Melzer, A. Onic, and M. Huemer, "On the sensitivity degradation caused by short-range leakage in FMCW radar systems," in *Lecture Notes Comput. Sci. (LNCS): Comput. Aided Syst. Theory – EUROCAST*, Las Palmas de Gran Canaria, Spain, Feb. 2015.

[14] Phase noise measurement solutions selection guide, Keysight Technologies, 2014.

[15] H. Gheidi and A. Banai, "Phase-noise measurement of microwave oscillators using phase-shifterless delay-line discriminator," *IEEE Trans. Microw. Theory Tech.*, vol. 58, no. 2, pp. 468–477, Feb. 2010.

[16] W. Khalil, B. Bakkaloglu, and S. Kiaei, "A self-calibrated on-chip phase-noise measurement circuit with -75 dBc single-tone sensitivity at 100 kHz offset," *IEEE J. Solid-State Circuits*, vol. 42, no. 12, pp. 2758–2765, Dec. 2007.

[17] A. Melzer, F. Starzer, H. Jäger, and M. Huemer, "On-chip delay line for extraction of decorrelated phase noise in FMCW radar transceiver MMICs," in *Proc. 23rd Austrian Workshop Microelectron. (Austrochip)*, Vienna, Austria, Sep. 2015.

[18] S. Kay, *Intuitive Probability and Random Processes using MATLAB*. New York, NY, USA: Springer, 2006.

[19] R. Feger, C. Wagner, S. Schuster, S. Scheiblhofer, H. Jäger, and A. Stelzer, "A 77-GHz FMCW MIMO radar based on an SiGe single-chip transceiver," *IEEE Trans. Microw. Theory Tech.*, vol. 57, no. 5, pp. 1020–1035, May 2009.

[20] B. Analui and A. Hajimiri, "Statistical analysis of integrated passive delay lines," in *Proc. IEEE Custom Integrated Circuits Conf.*, Sep. 2003, pp. 107–110.

Alexander Melzer was born in Voitsberg, Austria, in 1988. He received his Dipl.-Ing. in Telematics from Graz University of Technology in December 2012. From 2013–2014 he was with Maxim Integrated Austria. Since March 2014, he has been a member of the Institute of Signal Processing at the Johannes Kepler University of Linz. Currently, he is working towards his Ph.D. in cooperation with DICE Danube Integrated Circuit Engineering GmbH. His research focuses on digital signal processing algorithms for automotive radar systems.

Alexander Onic is Concept Engineer for automotive Radar at Infineon Technologies in Linz, Austria. He received the doctoral degree from Alpen-Adria-Universität Klagenfurt in 2013, where he was part of the research team that invented Unique Word OFDM, a novel signaling scheme for digital communication, under supervision of Mario Huemer. In 2007, he graduated with the Dipl.-Ing. degree from Friedrich-Alexander-Universität Erlangen-Nürnberg, after studying electrical engineering with an emphasis on information technology and signal processing. Alex' research interest in signal processing, communication engineering and estimation theory is consequently supplemented by the research cooperation of Infineon and Johannes-Kepler-Universität Linz on radar signal processing topics.

Florian Starzer was born in Steyr, Austria, and is currently Concept Engineer for automotive radar systems at DICE GmbH & Co KG in Linz, Austria. He received his doctoral degree from the University of Linz in 2013 where he worked on concepts and circuits for low-noise automotive radar sensor transmitters. He received his Dipl.-Ing. (FH) degree from the University of applied sciences after studying hardware software systems engineering, focusing on low-power digital circuits. His current focus lies in computational efficient behavioral modelling of radar's RF circuits.

Mario Huemer (SM'07) was born in Wels, Austria, in 1970. He received the Dipl.-Ing. degree in mechatronics and the Dr.techn. (Ph.D.) degree from the Johannes Kepler University of Linz, Austria, in 1996 and 1999, respectively. From 1997 to 2000, he was a Research Assistant at the Institute for Communications and Information Engineering at the University of Linz, Austria. From 2000 to 2002, he was with Infineon Technologies Austria, research and development center for wireless products. From 2002–2004 he was a Lecturer at the University of Applied Sciences of Upper Austria, and from 2004–2007 he was Associate Professor for Electronics Engineering at the University of Erlangen-Nuremberg, Germany. In 2007 he moved to Klagenfurt, Austria, to establish the Chair of Embedded Systems and Signal Processing at Klagenfurt University as a Full Professor. From 2012 to 2013 he served as dean of the Faculty of Technical Sciences. Since September 2013 he is head of the newly founded Institute of Signal Processing at the Johannes Kepler University of Linz, Austria. His research interests are adaptive and statistical signal processing, signal processing architectures and implementations, as well as mixed signal processing with applications in communications, radio frequency and baseband integrated circuits, battery- and power management for mobile devices, and sensor signal processing. Within these fields he published more than 160 papers. In 2000 he received the German ITG and the Austrian GIT award for dissertations, and in 2010 the Austrian Kardinal Innitzer award in natural sciences. His review work includes national and European research projects as well as international journals. Since 2009 he is member of the editorial board of the *International Journal of Electronics and Communications (AEUE)*.

Mario Huemer is member of the IEEE, the German Society of Information Technology (ITG), and the Austrian Electrotechnical Association (OVE).